Supporting Information for

Enhanced surface reconstruction of V-Doped Ni_3N driven by strong OH adsorption to boost 5-hydroxymethylfurfural electrooxidation for energy-saving H_2 production

Qi Zhou, Juan Wang, Ga Jin, Huiling Liu*, Cheng Wang

Institute for New Energy Materials and Low-Carbon Technologies, School of Materials Science and Engineering, Tianjin Key Laboratory of Advanced Functional Porous Materials, Tianjin University of Technology, Tianjin, 300384, China

Description: There are 16 pages in the Supporting Information, including 26 figures and 2 tables.

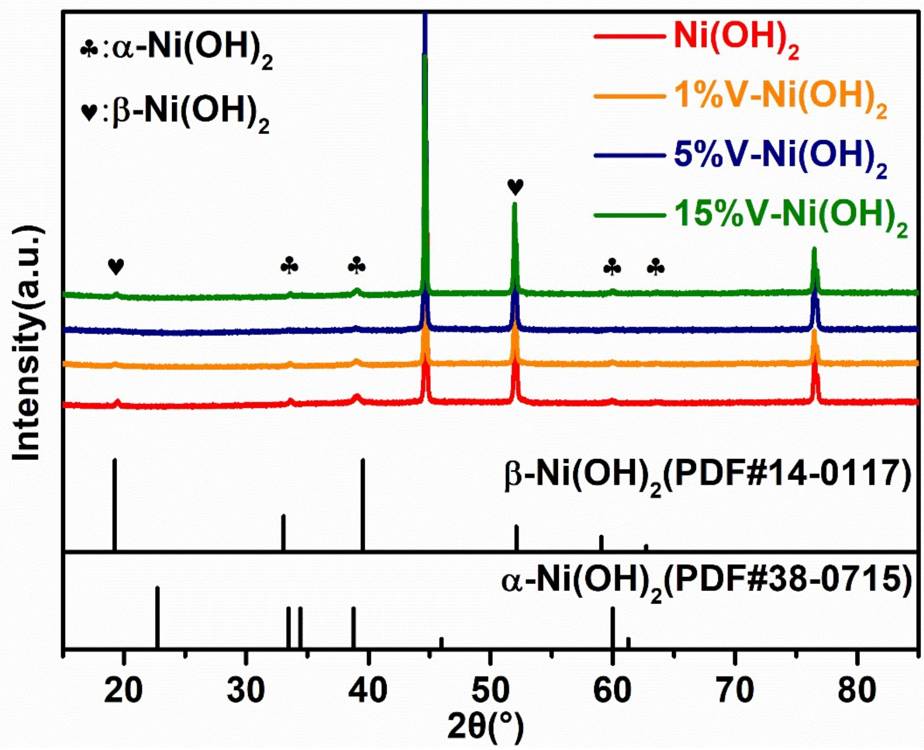

Fig. S1 XRD patterns of the $Ni(OH)_2$, 1%V-, 5%V- and 15%V-$Ni(OH)_2$.

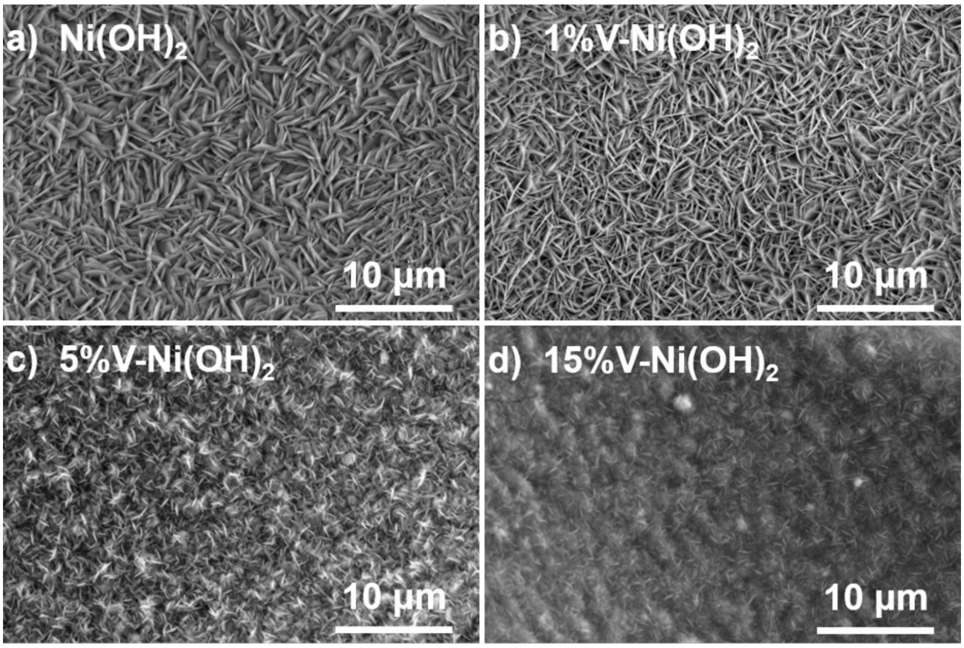

Fig. S2 SEM images of (a) $Ni(OH)_2$, (b) 1%V-$Ni(OH)_2$, (c) 5%V-$Ni(OH)_2$ and (d) 15%V-$Ni(OH)_2$.

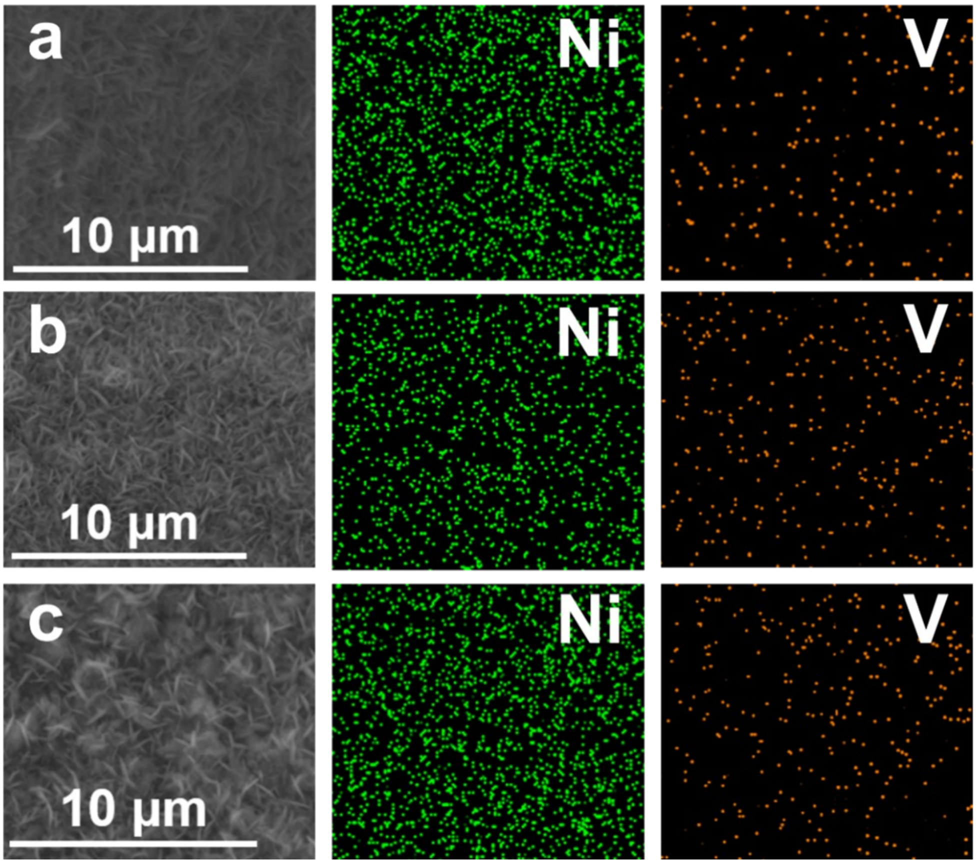

Fig. S3 Elemental mapping images of Ni and V for (a) 1%V-$Ni(OH)_2$, (b) 5%V-$Ni(OH)_2$ and (c) 15%V-$Ni(OH)_2$.

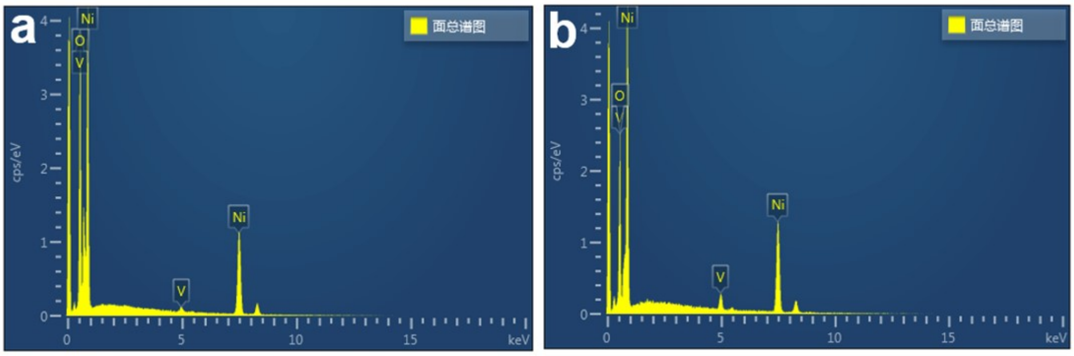

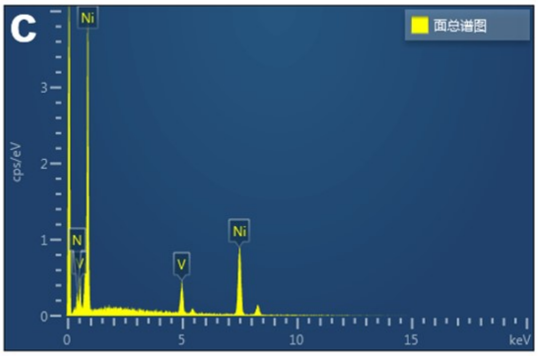

d Samples	Atomic Fraction (%)		The ratio of V/Ni
	Element Ni	Element V	
1%V-$Ni(OH)_2$	98.17	1.83	1.86/100
5%V-$Ni(OH)_2$	94.16	5.84	6.2/100
15%V-$Ni(OH)_2$	86.51	13.49	15.6/100

Fig. S4 EDX spectra of (a) 1%V-$Ni(OH)_2$, (b) 5%V-$Ni(OH)_2$ and (c) 15%V-$Ni(OH)_2$. (d) Corresponding atomic ratios of V to Ni for different samples.

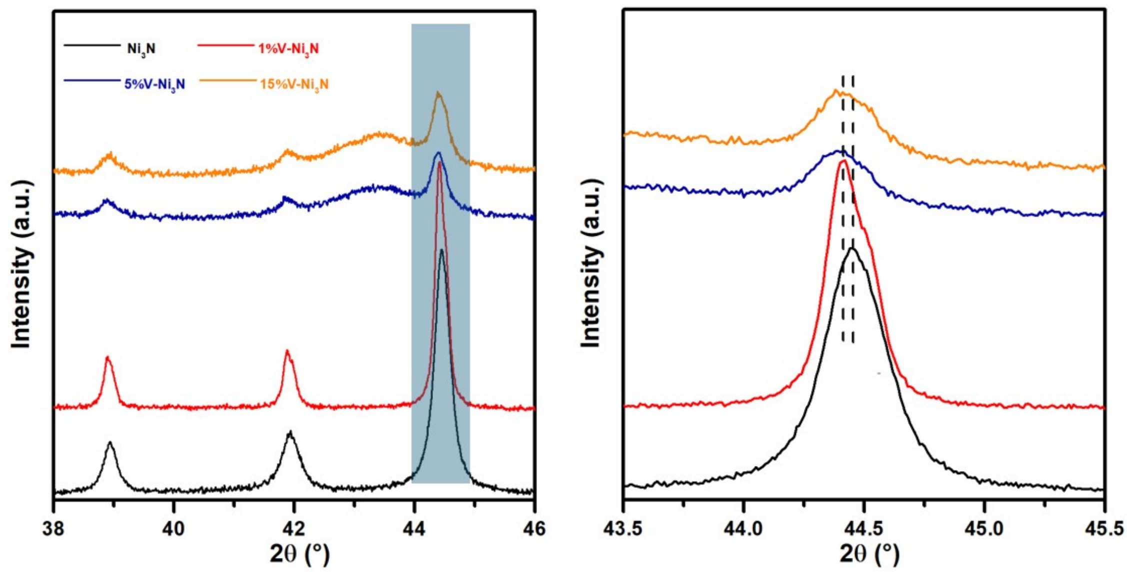

Fig. S5 XRD patterns of the Ni_3N and 1%, 5%,15%V-Ni_3N powder samples.

Samples	Atomic Fraction (%)		The ratio of V/Ni
	Element Ni	Element V	
1%V-Ni_3N	99.5	0.5	0.50/100
5%V-Ni_3N	94.0	6.0	6.38/100
15%V-Ni_3N	84.4	15.6	18.48/100

Fig. S6 The atomic ratios of V to Ni for different samples determined by EDX.

Samples	Atomic Fraction (%)		The ratio of V/Ni
	Element Ni	Element V	
1%V-Ni_3N	99.2	0.8	0.80/100
5%V-Ni_3N	93.9	6.1	6.51/100
15%V-Ni_3N	82.9	17.1	20.51/100

Fig. S7 The atomic ratios of V to Ni for different samples determined by ICP.

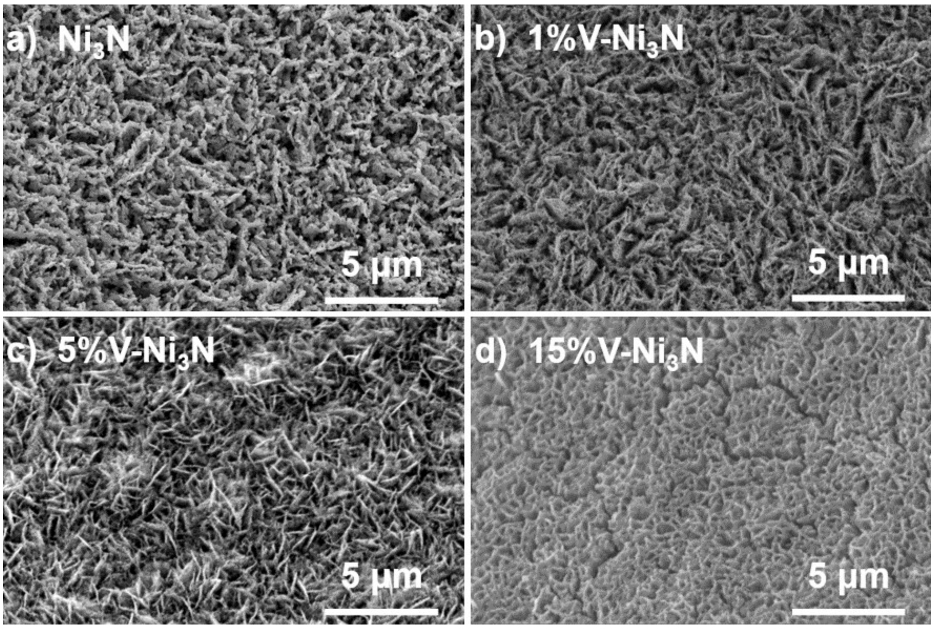

Fig. S8 SEM images of (a) Ni_3N, (b) 1%V-Ni_3N, (c) 5%V-Ni_3N and (d) 15%V-Ni_3N.

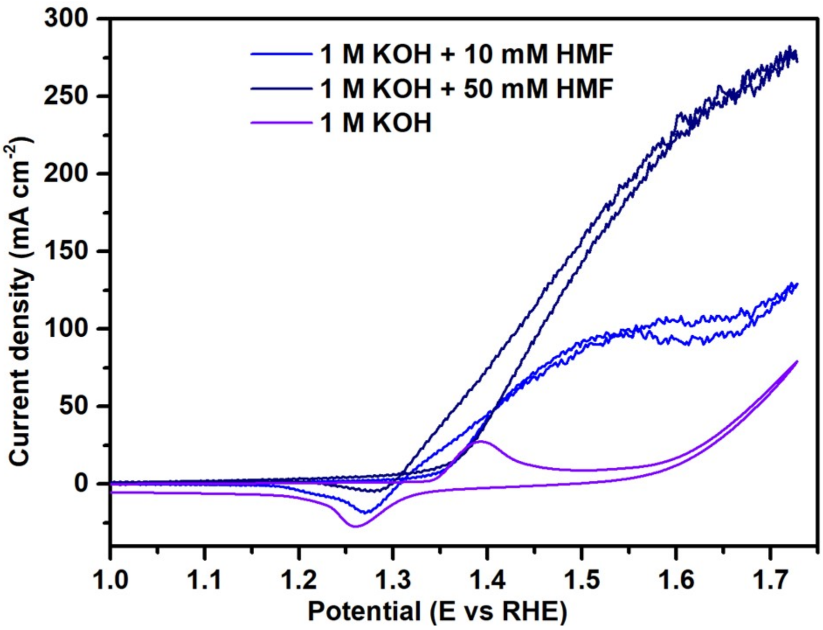

Fig. S9 CV curves of the 5%V-Ni_3N in 1.0 M KOH with and without 10/50 mM HMF at a scan rate of 10 mV s^{-1}. In 1.0 M KOH without HMF, the redox peaks are ascribed to the redox between Ni^{2+} and Ni^{3+}. The increase in current after 1.6 V is due to the start of oxygen evolution reaction. In the presence of 10 mM HMF, the anodic current starts to increase at the same position (1.35 V) with that in the purple line, indicating the oxidation of Ni^{2+} to Ni^{3+}. Then the current rapidly increases as the oxidation reaction of HMF. At around 1.55-1.65 V, the current shows a slight decrease because of the consumption of HMF. The decrease in the current is avoided when the HMF concentration is 50 mM (black line). The following increase in the current after 1.65 V is due to the competed OER. During cathodic sweep, the peak belongs to the reduction of Ni^{3+} to Ni^{2+}.

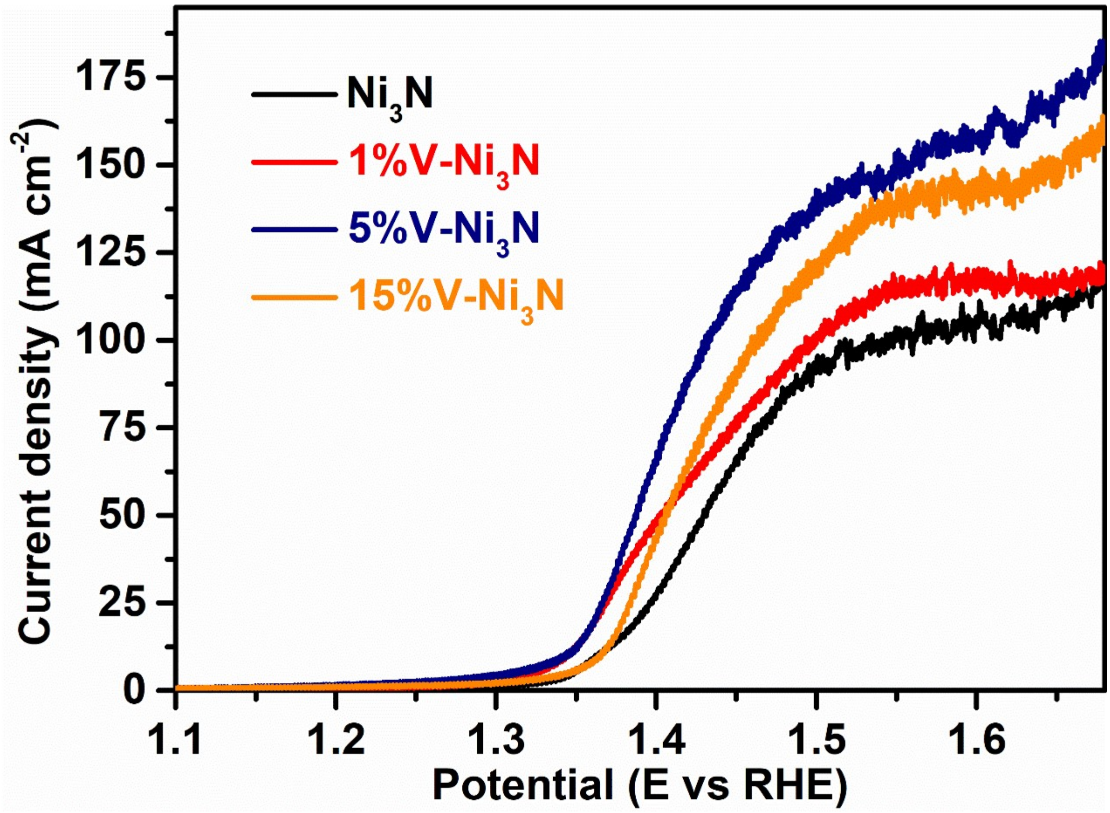

Fig. S10 LSV curves of HMFOR on V-Ni_3N with different doping ratios.

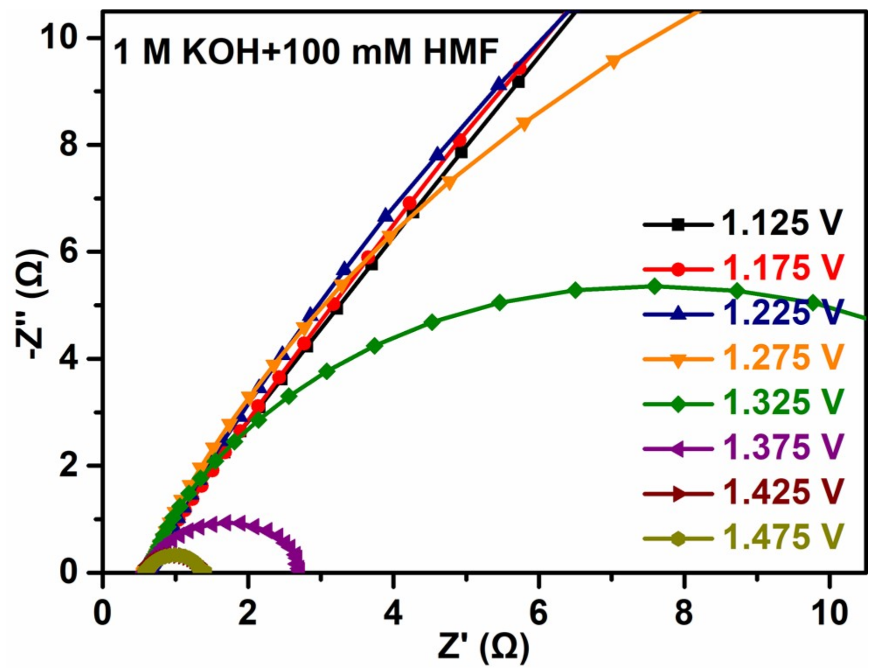

Fig. S11 In situ Nyquist plots of the Ni_3N for HMFOR.

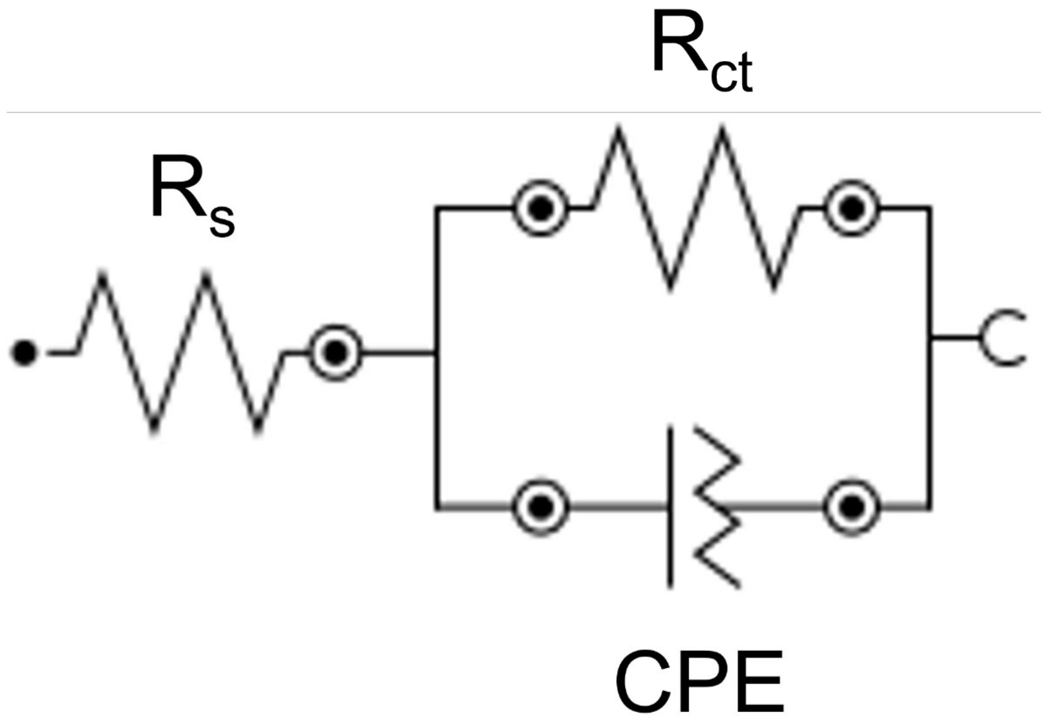

Fig. S12 The corresponding equivalent circuit diagram consisting of an electrolyte resistance (R_s), a charge transfer resistance (R_{ct}), and a constant phase element (CPE).

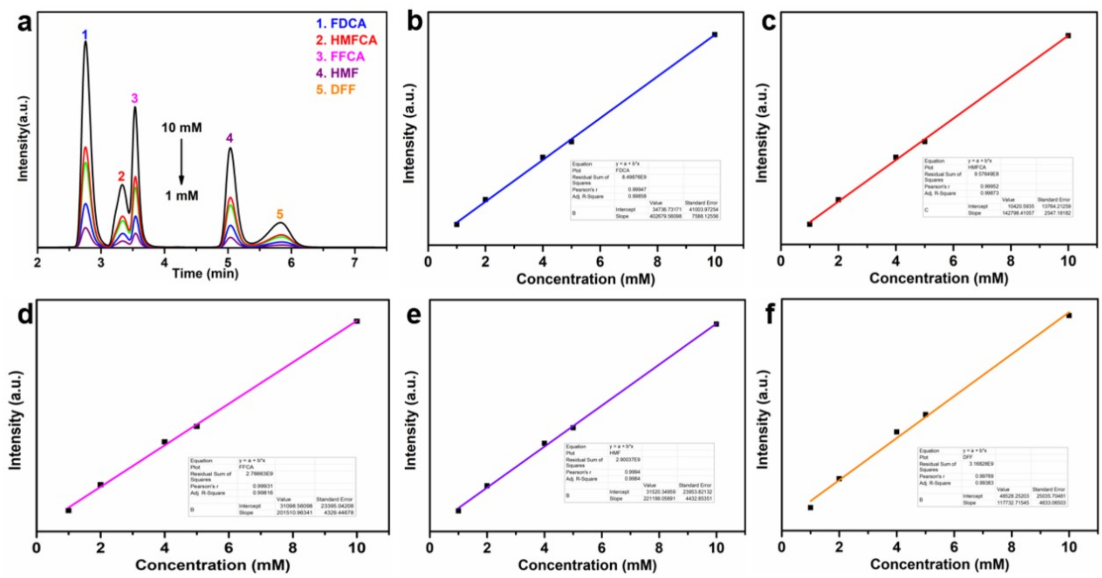

Fig. S13 (a) Reference HPLC spectra, and calibration curves for (b) FDCA, (c) HMFCA, (d) FFCA, (e) HMF, and (f) DFF.

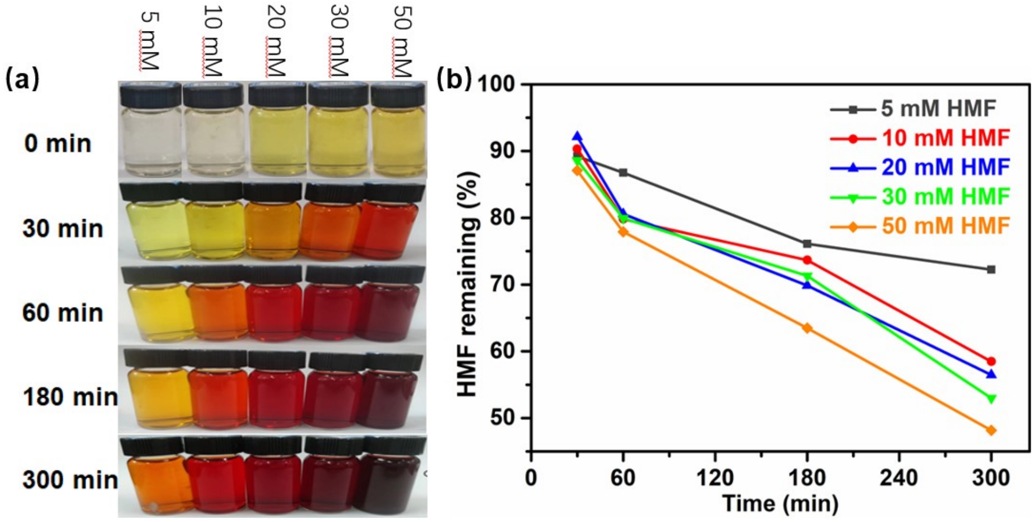

Fig. S14 (a) Photographs of 1 M KOH with 5/10/20/30/50 mM HMF under different standing time. (b) HMF remaining (%) determined by HPLC.

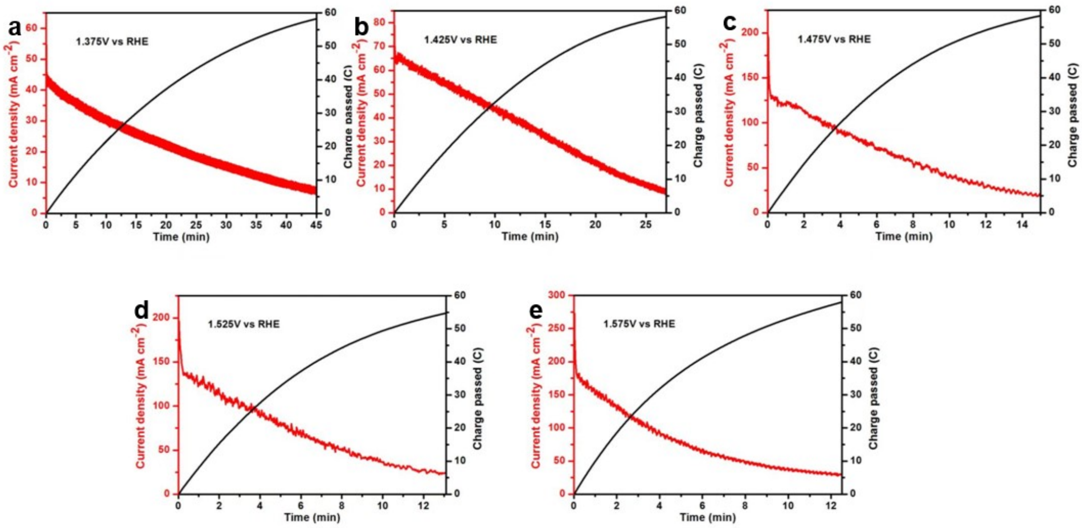

Fig. S15 The current density and charge versus electrooxidation time at (a) 1.375 V, (b) 1.425 V, (c) 1.475 V, (d) 1.525 V, (e) 1.575 V.

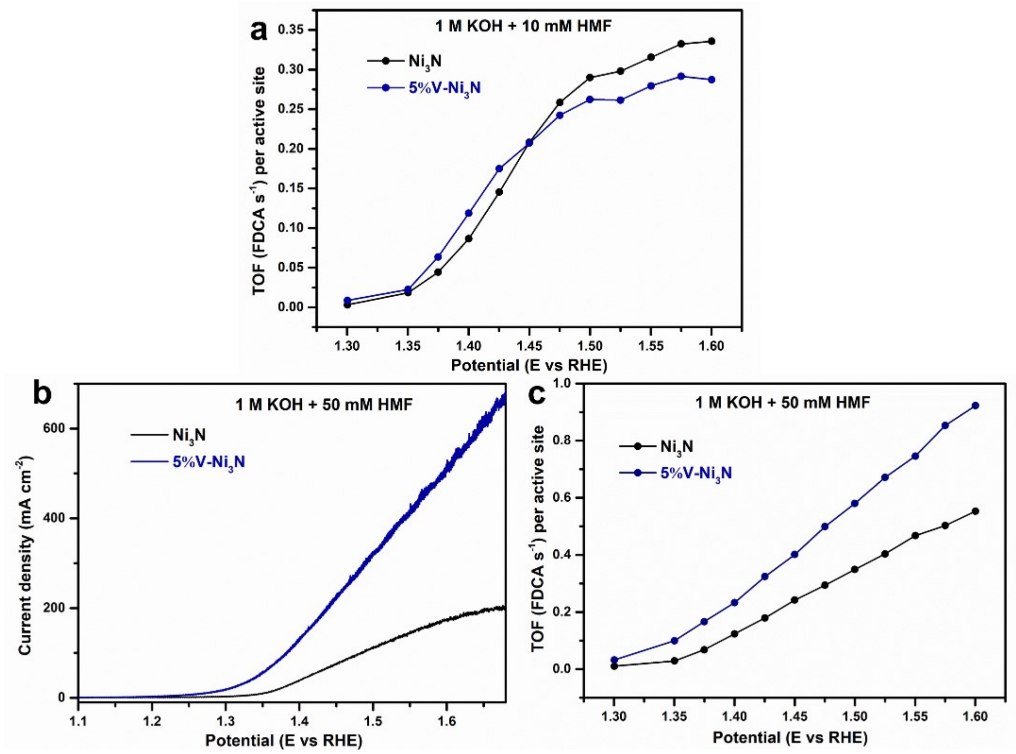

Fig. S16 (a) TOFs of Ni_3N and 5%V-Ni_3N for HFMOR with 10 mM HMF at different applied potentials. (b) LSV curves of Ni_3N and 5%V-Ni_3N for HFMOR with 50 mM HMF. (c) TOFs of Ni_3N and 5%V-Ni_3N for HFMOR with 10 mM HMF at different applied potentials.

The TOFs for HMFOR and HER were calculated according to the equations below:

$$TOF = \frac{total\ product\ turn\ overs\ /\ cm^2\ geometric\ area}{activesites\ /\ cm^2\ geometric\ area}$$

$$Product(FDCA) = \left(j\frac{mA}{cm^2}\right)\left(\frac{1\ C\ s^{-1}}{1000\ mA}\right)\left(\frac{1\ mol\ e^-}{96485\ C}\right)\left(\frac{1\ mol\ FDCA}{6\ mol\ e^-}\right)\left(\frac{6.022\times10^{23}\ FD}{1\ mol\ F}\right. = 1.04\times10^{15}\frac{FDCA/s}{cm^2}per\frac{mA}{cm^2}$$

$$Product(H_2) = \left(j\frac{mA}{cm^2}\right)\left(\frac{1\ C\ s^{-1}}{1000\ mA}\right)\left(\frac{1\ mol\ e^-}{96485\ C}\right)\left(\frac{1\ mol\ H_2}{2\ mol\ e^-}\right)\left(\frac{6.022\times10^{23}\ H_2\ m}{1\ mol\ H_2}\right. = 3.12\times10^{15}\frac{H_2/s}{cm^2}per\frac{mA}{cm^2}$$

$$activesites = \left(\frac{number\ of\ atoms/\ unit\ cell}{volume/\ unit\ cell}\right)^{\frac{2}{3}}$$

$$A_{ECSA}^{Ni_3N} = \frac{Cdl_{Ni_3N}}{Cs}$$

$$A_{ECSA}^{NiOOH} = \frac{Cdl_{NiOOH}}{Cs}$$

The plot of current density can be converted into a TOF plot according to:

$$TOF_{FDCA} = \frac{1.04 \times 10^{15} \frac{FDCA/s}{cm^2} per \frac{mA}{cm^2} \times |j|}{activesites \times A_{ECSA}}$$

$$TOF_{H_2} = \frac{3.12 \times 10^{15} \frac{H_2/s}{cm^2} per \frac{mA}{cm^2} \times |j|}{activesites \times A_{ECSA}}$$

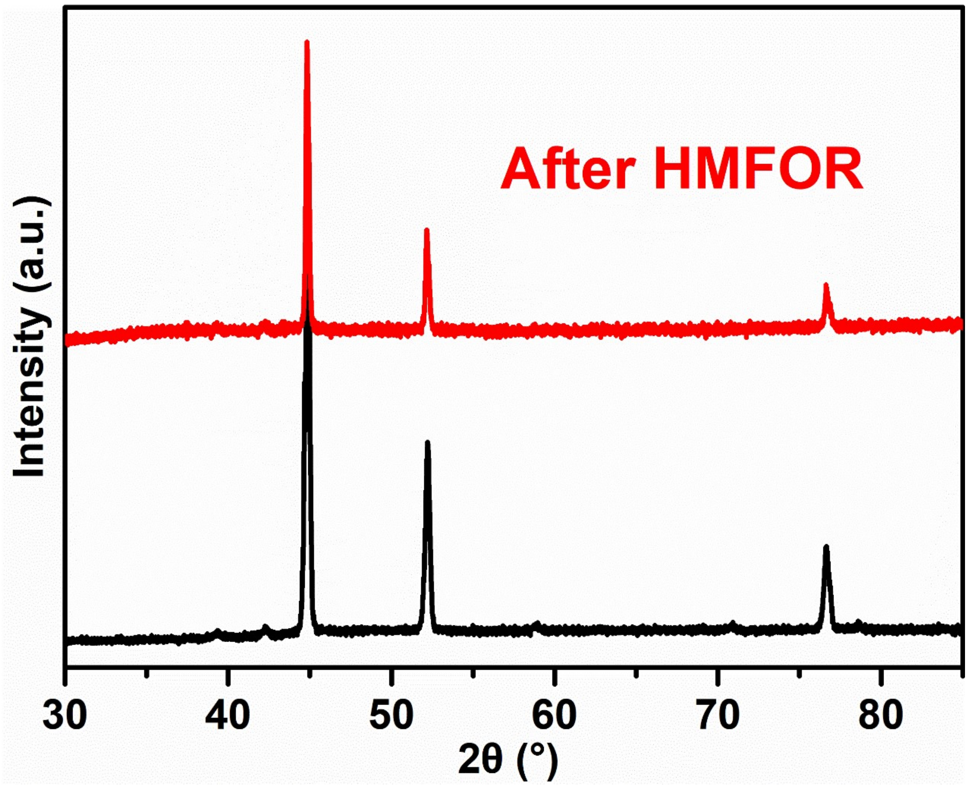

Fig. S17 XRD patterns of 5%V-Ni_3N before and after HMFOR.

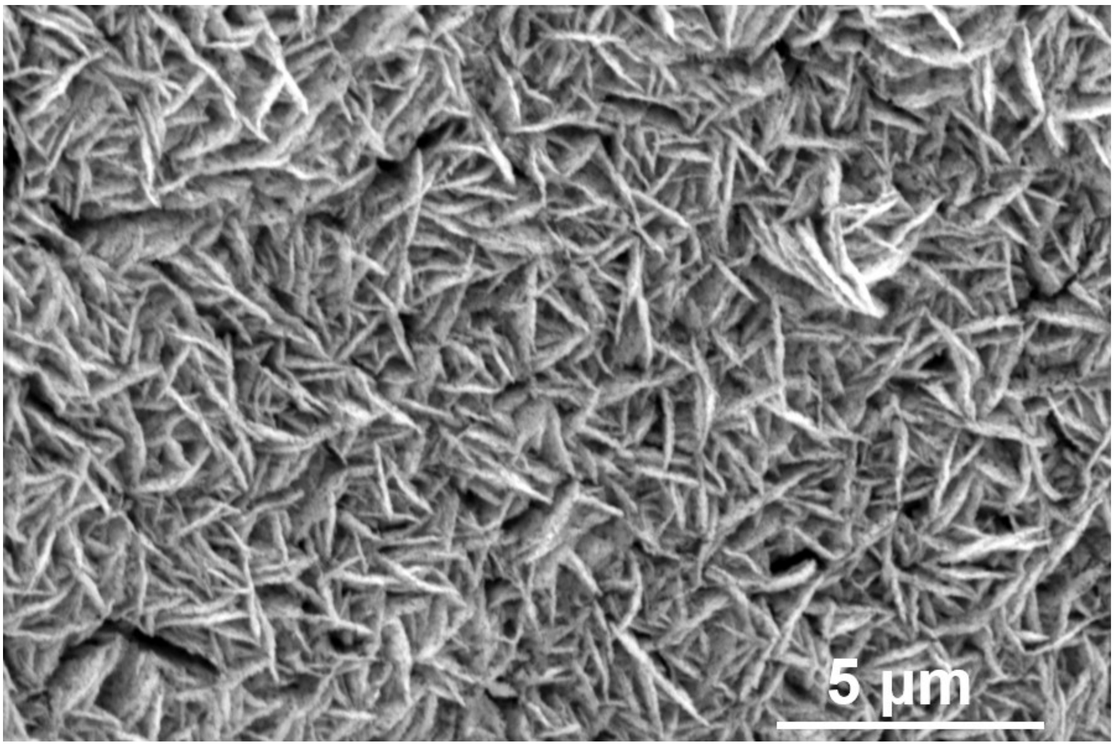

Fig. S18 SEM image of 5%V-Ni_3N after HMFOR.

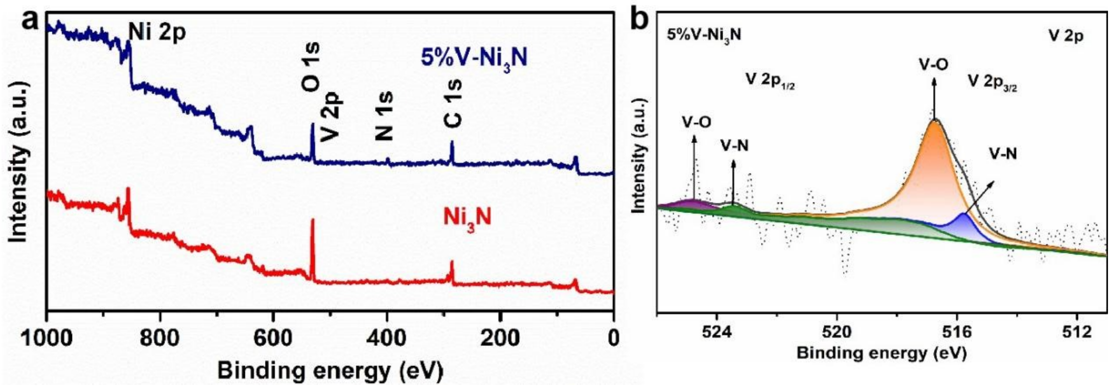

Fig. S19 (a) Survey XPS spectra of Ni_3N and 5%V-Ni_3N. (b) V 2p XPS spectra of 5%V-Ni_3N before and after HMFOR.

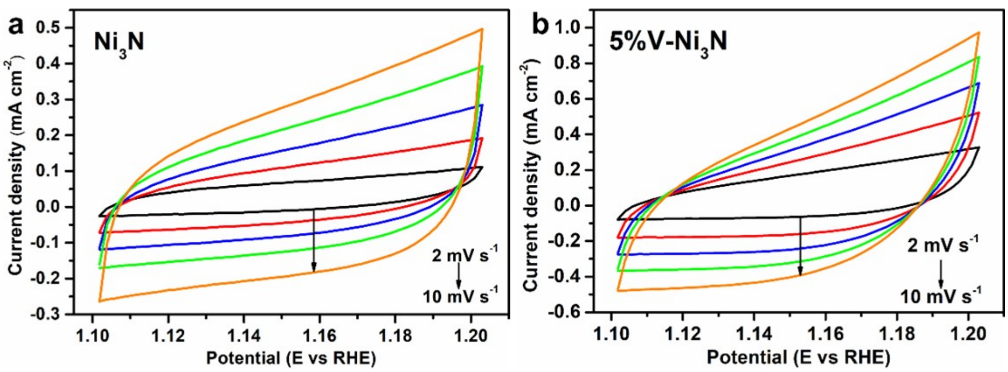

Fig. S20 CV curves of (a) Ni_3N and (b) 5%V-Ni_3N in 1 M KOH at different scan rates.

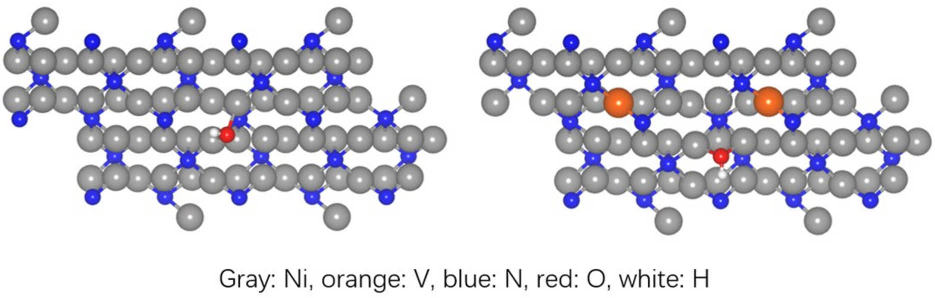

Fig. S21 DFT-optimized models of OH adsorption on Ni_3N and 5%V-Ni_3N.

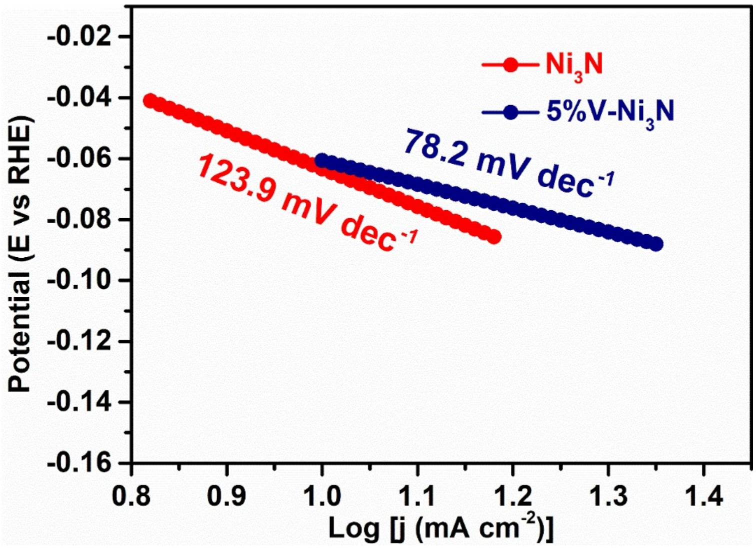

Fig. S22 Tafel slopes of the HER processes on the 5%V-Ni_3N and Ni_3N.

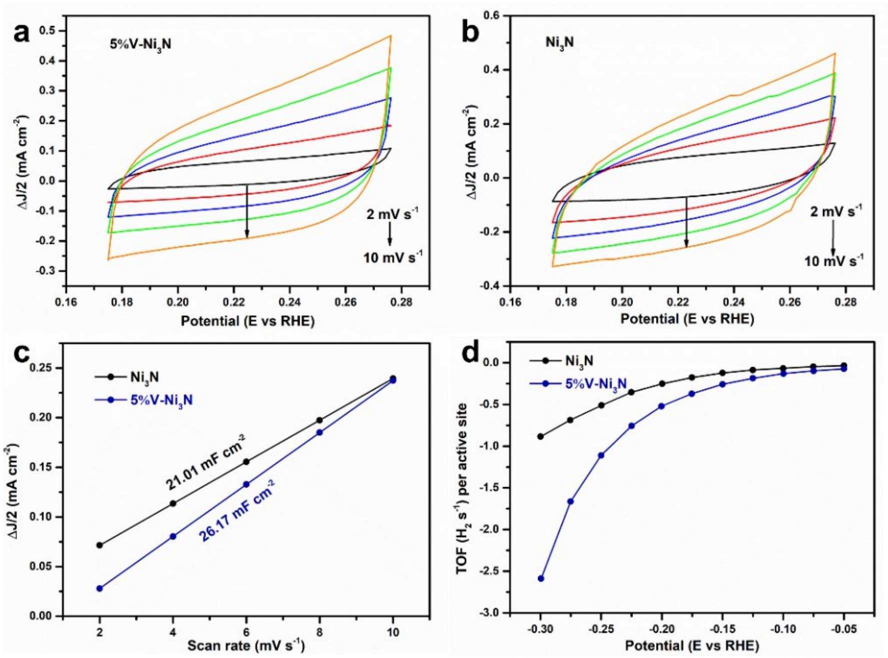

Fig. S23 CV curves of (a) 5%V-Ni_3N and (b) Ni_3N in 1.0 M KOH with different scanning rates. (c) C_{dl} of Ni_3N and 5%V-Ni_3N. (d) TOFs of Ni_3N and 5%V-Ni_3N for HER in 1.0 M KOH at different applied potentials.

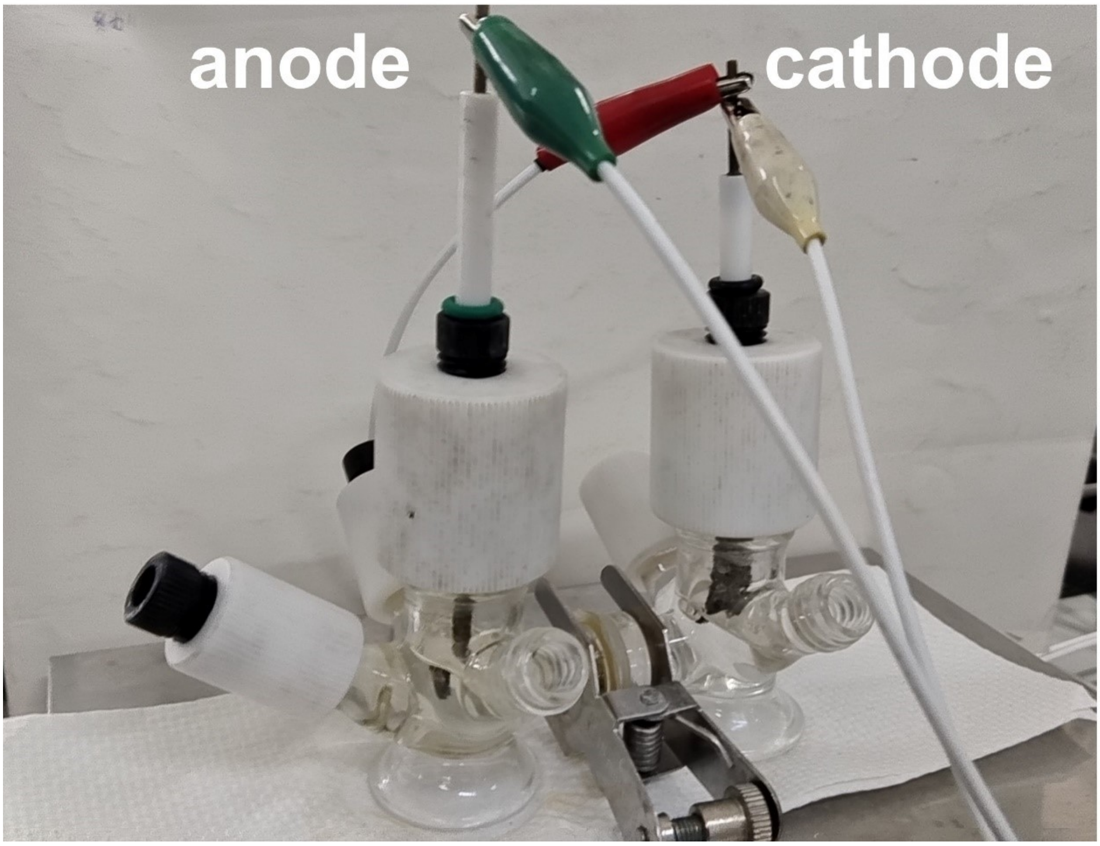

Fig. S24 Device diagram of HMFOR coupled with HER.

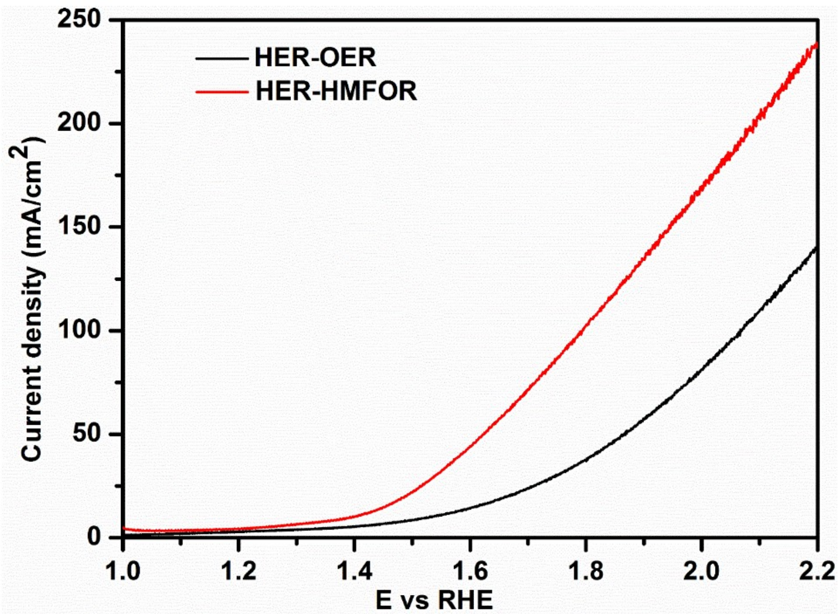

Fig. S25 LSV curves for HMFOR-HER and OER-HER with the 5%V-Ni_3N serving as both the anode and cathode in 1 M KOH with and without 100 mM HMF.

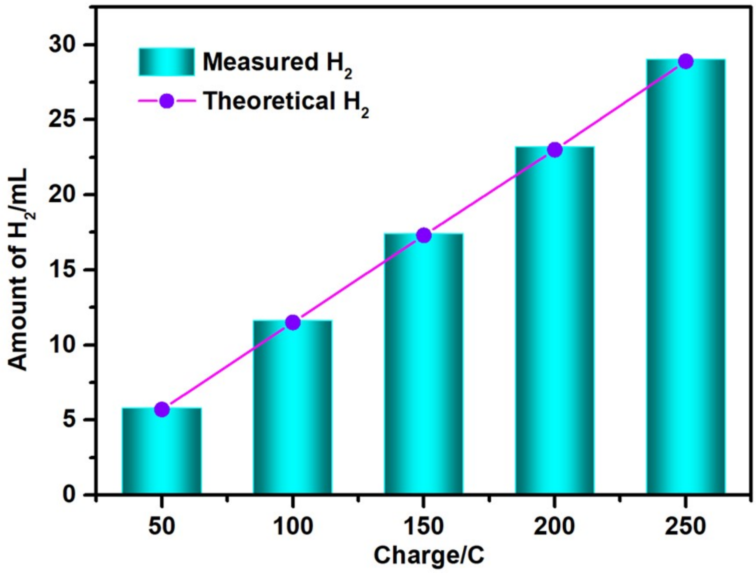

Fig. S26 Amounts of H_2 produced in the continuous HMFOR-HER system with 5%V-Ni_3N as the electrodes at different passing charge.

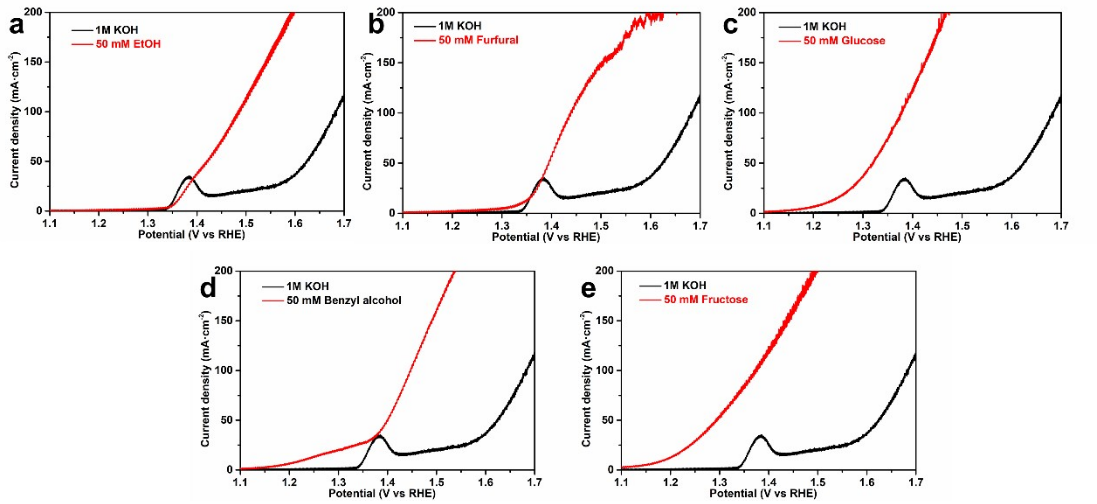

Fig. S27 LSV curves of the 5%V-Ni_3N in 1 M KOH with and without 50 mM ethanol, FF (furfural), glucose, BA (benzyl alcohol), fructose.

Table S1 The conversion, FE, yield and production rate of 5%V-Ni_3N at different potentials.

Potential (V vs RHE)	Conversion	FE	Yield	Production rate (μmol cm^{-2} h^{-1})
1.375	98%	98%	98%	139.3
1.425	99%	99%	99%	231.0
1.475	100%	98%	98%	403.1
1.525	100%	95%	96%	475.6
1.575	91%	81%	81%	489.7

Table S2 Comparisons of HMFOR electrocatalytic activity of 5%V-Ni_3N to other reported electrocatalysts in 1 M KOH and 10 mM HMF.

Electrode materials	Current density (mA cm^{-2})	Potential (V)	Yield	FE	Production rate (μmol cm^{-2} h^{-1})	Reference
5%V-Ni_3N	10 50	1.342 1.387	98%	98%	403 (1.475 V[a])	this work
Ni_3N	50	1.402	86%	80%	280 (1.475 V)	this work
Ni_3N@C	50	1.38	98%	99%		1
V_2O_3-Ni_3N	10	1.47	96%		66	2
Ni_2PNPA/NF	50	1.38	99%	99%	67 (1.423 V)	3
NiSe@NiO_x	50	1.36	99%	99%	100 (1.423 V)	4
Co_9S_8-Ni_3S_2@NSOC	10	1.33	98.8%	98.6%	105 (1.4 V)	5
NiCoMn-LDHs	50	1.61	91.7%	70%	55 (1.5 V)	6
Cu_xS@NiCo-LDH	87	1.3	99%	99%	80 (1.32 V)	7
$Ni(OH)_2$-PO_x	10	1.65	94.2%	93.5%	50 (1.464 V)	8
CoO-$CoSe_2$	50	1.4	99%	97.9%	100 (1.43 V)	9
MoO_2-FeP	10	1.359	98.6%	97.8%	80 (1.424 V)	10
NiCu NTs	100	1.58	99%	96%	105 (1.424 V)	11

CF-$Cu(OH)_2$	20	1.523	98.7%	98%	170 (1.723 V)	12
VN	10	1.36	96%	84%	110	13
Ni_xB/NF	55	1.45	98.5%	98.5%	200 (1.45 V)	14

a: All the potentials are referred to RHE.

References:

[1] N. Zhang, Y. Zou, L. Tao, W. Chen, L. Zhou, Z. Liu, B. Zhou, G. Huang, H. Lin and S. Wang, Angew. Chem., Int. Ed., 2019;58:15895-15903. https://doi.org/10.1002/anie.201908722

[2] S. Liang, L. Pan, T. Thomas, B. Zhu, C. Chen, J. Zhang, H. Shen, J. Liu and M. Yang, Chem. Eng. J., 2021, 415, 128864. https://doi.org/10.1016/j.cej.2021.128864

[3] B. You, N. Jiang, X. Liu and Y. Sun, Angew. Chem., Int. Ed., 2016;55:9913-9917. https://doi.org/10.1002/anie.201603798

[4] L. Gao, Z. Liu, J. Ma, L. Zhong, Z. Song, J. Xu, S. Gan, D. Han and L. Niu, Appl. Catal., B, 2020;261:118235. https://doi.org/10.1016/j.apcatb.2019.118235

[5] Y. Zhang, Z. Xue, X. Zhao, B. Zhang and T. Mu, Green Chem., 2022;24:1721-1731. https://doi.org/10.1039/D1GC04499K

[6] B. Liu, S. Xu, M. Zhang, X. Li, D. Decarolis, Y. Liu, Y. Wang, E. K. Gibson, C. R. A. Catlow and K. Yan, Green Chem., 2021;23:4034-4043. https://doi.org/10.1039/D1GC00901J

[7] X. Deng, X. Kang, M. Li, K. Xiang, C. Wang, Z. Guo, J. Zhang, X.-Z. Fu and J.-L. Luo, J. Mater. Chem. A, 2020;8:1138-1146. https://doi.org/10.1039/C9TA06917H

[8] X. Xu, X. Song, X. Liu, H. Wang, Y. Hu, J. Xia, J. Chen, M. Shakouri, Y. Guo and Y. Wang, ACS Sustain. Chem. Eng., 2022;10:5538-5547. https://doi.org/10.1021/acssuschemeng.2c00121

[9] X. Huang, J. Song, M. Hua, Z. Xie, S. Liu, T. Wu, G. Yang and B. Han, Green Chem., 2020;22:843-849. https://doi.org/10.1039/C9GC03698A

[10] G. Yang, Y. Jiao, H. Yan, Y. Xie, A. Wu, X. Dong, D. Guo, C. Tian and H. Fu, Adv. Mater., 2020;32:e2000455. https://doi.org/10.1002/adma.202000455

[11] L. Zheng, Y. Zhao, P. Xu, Z. Lv, X. Shi and H. Zheng, J. Mater. Chem. A, 2022;10:10181-10191. https://doi.org/10.1039/D2TA00579D

[12] X. Pang, H. Bai, H. Zhao, W. Fan and W. Shi, ACS Catal., 2022;12:1545-1557. https://doi.org/10.1021/acscatal.1c04880

[13] S. Li, X. Sun, Z. Yao, X. Zhong, Y. Cao, Y. Liang, Z. Wei, S. Deng, G. Zhuang, X. Li and J. Wang, Adv. Funct. Mater., 2019;29:1807031. https://doi.org/10.1002/adfm.201904780

[14] S. Barwe, J. Weidner, S. Cychy, D. M. Morales, S. Dieckhofer, D. Hiltrop, J. Masa, M. Muhler and W. Schuhmann, Angew. Chem., Int. Ed., 2018;57:11460-11464. https://doi.org/10.1002/anie.201806298